THE ASTROPHYSICAL JOURNAL, 463:797–807, 1996 June 1


# DOUBLE-GAUSSIAN MODELS OF BRIGHT POINTS OR WHY BRIGHT POINTS ARE USUALLY DARK

A. M. TITLE
Lockheed Palo Alto Research Laboratory, Department 91-39 3251 Hanover Street, Palo Alto, CA 94304
AND
T. E. BERGER
Center for Space Science and Astrophysics, ERL 328, Stanford University, Stanford, CA 94305
*Received 1995 September 8; accepted 1995 December 5*

## ABSTRACT

We have modeled the structure of small bright features, "bright points" seen in an outstanding CH filter (G-band) image. In our model, bright points consist of a Gaussian bright core centered in a Gaussian dark surround. The basis for this approach is the observation that nearly all of the bright points in the image exist within intergranular lanes, vertices between granules, or local brightness depressions. Using reasonable estimates for the size and depth of vertices and lanes, the model predicts that bright points clearly detectable in images with 0".2 resolution will seldom be detectable in images with resolutions beyond 0".4. This occurs because the transfer function of the telescope and atmosphere averages the bright points with their comparably sized dark surroundings to near zero contrast when blurred beyond 0".4. These results explain the great rarity of images that clearly show bright points. Furthermore, the image shows many bright points with core diameters equal to that of the FWHM of a point-spread function of a perfect telescope. If the intensity profiles of these bright points were Gaussian on a flat background, then their intrinsic brightness would have to be unrealistically high and they would not disappear on images blurred beyond 0".4, but would simply gradually expand in size and drop in contrast as the blur increased. Because the bright points are sites of magnetic fields, our model helps to explain lower resolution disk center observations that show magnetic fields occur in regions that are dark relative to the mean continuum level. The modeling also suggests that bright points with diameters of 0".1 or less would be undetectable in the current generation of 0.5 m high-resolution solar telescopes, under any seeing conditions.

*Subject headings:* Sun: activity — Sun: granulation — Sun: photosphere — techniques: image processing

## 1. INTRODUCTION

On the very best continuum images of the quiet Sun, it is possible to identify small, bright, relatively long-lived structures that have characteristics significantly different from granulation. These structures are found within active regions and in the supergranulation network of the quiet Sun, and have been termed facular and network bright points, respectively. Early observations of facular bright points (Dunn, Mann, & Simon 1973; Dunn & Zirker 1974; Mehltretter 1974) established that their typical size is below 0".5 and that they are often found among larger filamentary structures, termed filigree. Richard Muller and his colleagues at the Pic-du-Midi Observatory have done the pioneering work of characterizing the quiet-Sun network bright points using their 48 cm refractor telescope (Muller & Keil 1983; Muller 1985; Muller et al. 1994). Although there is evidence that facular and network bright points may have different size distributions (Muller et al. 1994), it is generally accepted that both are manifestations of the same physical phenomenon; namely, small-scale magnetic flux tubes in the lower photosphere. This association has as its basis the coincidence of line-center brightening in spectroheliograms and magnetograms (Sheeley 1969; Chapman & Sheeley 1968). Chapman (1970) also established that facular and network bright points exhibit high contrast at disk center when imaged in the violet bandhead of the CN radical (3883 Å). Muller (1985) later discovered that bright points are well visible at all points on the disk in wideband observations in the Fraunhofer G band due to the 4300 Å bandhead of CH.

We have used a 12 Å bandpass G-band filter (4305 Å center) in conjunction with Ca II K line, magnetograms, and continuum observations at the Swedish Solar Observatory on La Palma to study bright point structure, evolution, and relation to magnetic fields. The first results (Berger et al. 1995a) describe the size, brightness, and spatial distribution statistics of G-band bright points at disk center. The brightest points exhibit 75% contrast relative to the quiet Sun near disk center and the smallest have a half-width at half-maximum (HWHM) of 0".09. Berger et al. (1994) show that bright points occur virtually without exception at sites of magnetic field flux in the photosphere, in confirmation of previous observations (Title et al. 1992, Zhang & Engvold 1993). In addition, the best G-band images show that the filigree is often just resolvable as chains of individual bright points, as inferred by deBoer & Kneer (1992) from speckle techniques.

The modal contrast at the center of a bright point is about 29% with respect to the mean quiet Sun in the best G-band images (Berger et al. 1995a), which makes their rarity in only slightly poorer seeing peculiar. One would expect that if the bright points had a Gaussian contrast profile, their contrast would drop not much faster than the square of the ratio of the resolution in the poorer frame to that in the better frame. Even in the case that the resolution in the best frame was 0".20 and the seeing in the poorer frame was 0".5, the contrast of the brightest points would drop to about 5%, which could still be easily observed. However, bright points are almost never recognized in 0".5 images. This has led us to examine the effects of seeing on

the appearance of the bright point and its immediate surroundings.

The intrinsic properties of an object of known functional form can be obtained in principle by deconvolving the point-spread function (PSF) of the telescope plus atmosphere from an image of the object. The PSF of the atmosphere and telescope can be approximated as a Gaussian function (somewhat better agreement with the seeing PSF can be achieved by two Gaussians: one to fit the core of the blurring function and another fit to the much broader scattered-light component). If the observed image consists of an ensemble of Gaussian-shaped intensity structures with a limited range in brightness, the effect of the telescope and atmosphere can be calculated and the original target largely recovered, if the noise level is low. This approach has been used for simplicity in past investigations of bright points (Mehltretter 1974; Spruit & Zwaan 1981; Muller & Keil 1983). The assumption of a Gaussian structure is reasonable for stars that are point objects in a uniform dark field, but, as we will show below, it is not valid for bright solar structures that are embedded in a locally depressed background.

The convolution of a Gaussian with a Gaussian is another Gaussian, whose width is the square root of the sum of the squares of the widths of the two. However, the width of a function after the convolution with a Gaussian is not necessarily different than before. For example, a single spatial frequency sine wave, when convolved with a Gaussian or any other real positive function, yields the same frequency sine wave. The two-dimensional functional form, which has the sine wave's shape invariance under convolution with cylindrically symmetric PSFs, is the Bessel function $J_0(kr)$. Bright points exist in dark intergranular areas, and the combination of the two profiles (bright core and dark surround) exhibit nearly the same width-preserving property as a $J_0(kr)$ profile.

Images of isolated bright points and modern MHD models of magnetic flux tubes both indicate that the continuum signature of a small flux tube is a bright core with a cooler dark surround (Knolker, Schussler, & Weisshaar 1988). However, low–spatial-resolution but high-precision photometric measurements of the continuum have indicated that the continuum is not brighter and is most probably slightly darker than the mean continuum intensity at sites of magnetic field (Hirayama, Hamana, & Mizugaki 1985; Nishikawa 1990; Nishikawa & Hirayama 1990). Comparison of high-resolution, nearly simultaneous continuum images and magnetograms taken at disk center also has shown that the sites of magnetic field are on average darker rather than brighter than the mean continuum for all values of magnetogram signal per pixel (Title et al. 1992; Topka, Tarbell, & Title 1992; Lawrence, Topka, & Jones 1993). These apparently contradictory results can be understood if the integrated intensity of a bright point and its dark surround is less than the mean continuum intensity at disk center and the magnetic field sites appear to be larger than their associated continuum locations.

In § 2, we briefly describe our observations. In § 3, we introduce the double-Gaussian (DG) contrast functions as models for bright points. We demonstrate the relative insensitivity of the observed HWHM and the high sensitivity of the contrast amplitude of DG bright points compared to pure Gaussian profiles under blurring. We examine the sensitivity of the deconvolved resolved central contrast to the observed parameters—the observed HWHM, the observed central contrast, and the observed minimum contrast. Then we briefly discuss how bright points appear in lanes. Finally, in § 4, we discuss some of the implications of the behavior of bright points with resolution and attempt to explain some past controversial observations.

## 2. OBSERVATIONS

Figure 1 shows an outstanding G-band image (12 Å filter centered at $\lambda 4305$), which was taken by G. Scharmer near disk center on 1993 September 20, at the Swedish Solar Observatory on La Palma, Spain, using a Kodak Megaplus 1.4 camera. The digital output of the camera was collected at the rate of 7 frames $s^{-1}$ on a Digital Equipment Corporation Alpha work station, and the best image in each 20 s interval was selected for recording using a real-time image-selection algorithm. The La Palma G-band subsystem is described in Berger et al. (1995a). Figure 2 shows a section of that image in positive (*left*) and negative (*right*) form. From the positive image it is clear that virtually all bright points occur in intergranular lanes. The negative image shows that nearly all bright points, which in the negative image appear as compact dark areas, have a surrounding bright ring. The dark areas around the bright points are much more obvious in the negative image.

## 3. BRIGHT POINT MODELS

### 3.1. *Definition of Double-Gaussian Model*

To model the contrast profile of the bright points, we represent the bright point contrast functions as the sum of centered, cylindrically symmetric Gaussians with positive and negative amplitudes.—double-Gaussian functions. Five parameters determine the model—the HWHMs, $a$ and $b$, and the contrast amplitudes $(\alpha + \delta)$ and $\delta$, of the positive core and the negative surround, and the HWHM of the PSF of the telescope and atmosphere, $c$. We approximate the telescope PSF by its best-fit Gaussian, allowing a simple addition in quadrature to combine HWHM values of the atmosphere and telescope PSF into a single-Gaussian function. The contrast of the tops of the granules in the immediate vicinity of a bright point is defined to be zero. The assumption that bright points are made of Gaussian shapes, and that the PSF function is also a Gaussian, results in considerable simplifications in the mathematical description of the effects of atmospheric and telescopic smearing, and allows insight into the principal parameters that effect the appearance of small structures.

As mentioned above, seeing is more accurately modeled as the sum of a Gaussian core that accounts for blurring and another wider Gaussian that accounts for scatter, but for the arguments used in this paper, inclusion of the scattering term would introduce complications and not much additional understanding. The role of the intergranular lane is another complication that a simple, cylindrically symmetric model neglects. The effect of lanes will be discussed further below. Initially, however, we will use the model to describe bright points that are at vertices in the granulation pattern rather than in lanes. In quiet Sun, most bright points are found in vertices in the granulation pattern that are most likely sink points in the granulation flow field. However, in regions of relatively high magnetic density—for example, the area shown in Figure 2—bright points are seen to accumulate in and often nearly fill lanes.

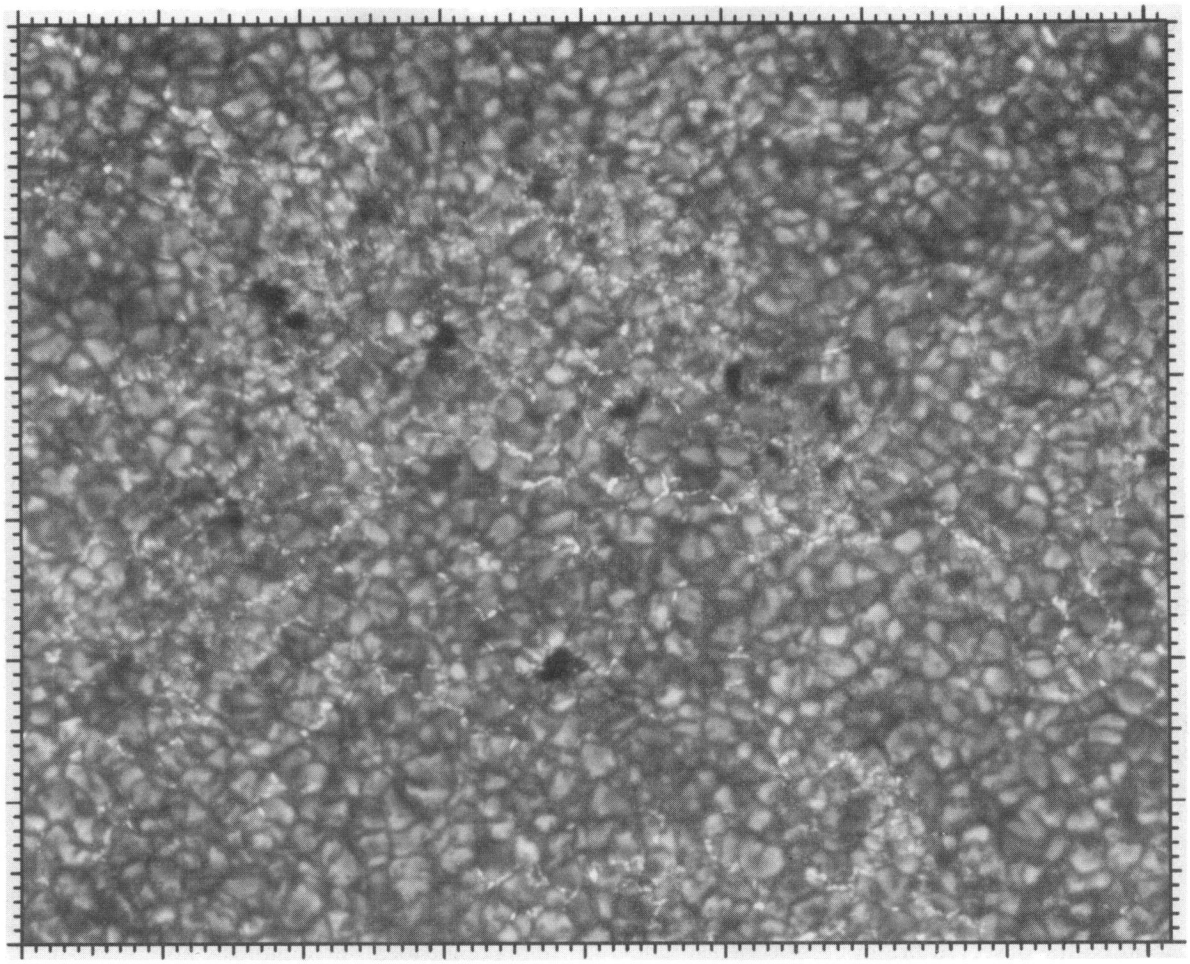

FIG. 1.—Image of the Sun taken in the G band at λ4305 at disk center on September 20 in NOAA 7581. The image is 65″ × 80″, and there are 15.92 pixels/arcsec.

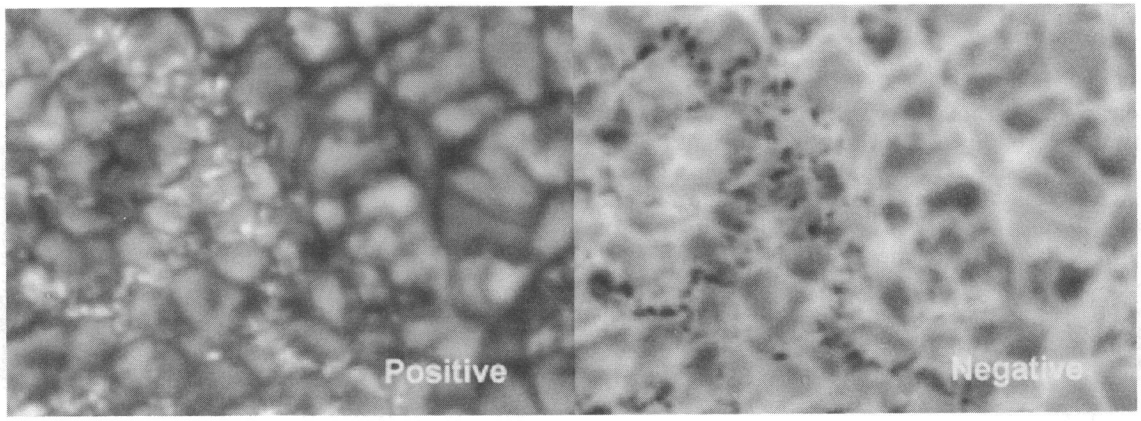


FIG. 2.—Portion of September 20 image in positive and negative. In the negative bright points appear as dark regions surrounded by bright rings.

We define a circular Gaussian function as

$$G(r, a) = 2^{-(r/a)^2}, \quad (1)$$

where $a$ is the HWHM. The area integral of $G(r, a)$ is

$$2\pi \int_0^\infty G(r, a) r\, dr = \frac{\pi a^2}{\ln 2}. \quad (2)$$

With this definition of the Gaussian function, the intrinsic DG function,

$$\mathrm{DG}_i(r, a, b, \alpha, \delta) = (\alpha + \delta)G(r, a) - \delta G(r, b), \quad (3)$$

where $a$ and $b$ are the widths and $(\alpha + \delta)$ and $\delta$ are the magnitudes of the core and surround Gaussians, respectively. Both magnitudes are defined to be positive, and $a < b$. The peak contrast of $\mathrm{DG}_i$ is $\alpha$.

The integrated contrast, the contribution of the bright point, and its surround to the solar luminosity is

$$2\pi \int_0^\infty \mathrm{DG}_r(r, a, b, \alpha, \delta) r\, dr = \frac{[(\alpha + \delta)a^2 - \delta b^2]\pi}{\ln 2} . \quad (4)$$

This integral is negative when

$$\frac{b^2}{a^2} > \frac{\alpha + \delta}{\delta} . \quad (5)$$

If we define a parameter $q$, where

$$\frac{\alpha}{\delta} = \frac{b^2 - a^2}{a^2}(q) , \quad (6)$$

then when $q < 1$, the integrated contrast will be negative. Because the unbounded integral of the bright point contrast is the same regardless of how the bright point is smeared, condition (6) is independent of the shape of the smearing function.

The $\mathrm{DG}_i$ contrast profile represents the actual contrast of the solar bright point and its immediate surroundings. However, it is not observed because of the combination of finite telescope resolution and atmospheric blurring. To account for these effects, we convolve the $\mathrm{DG}_i$ contrast function with the Gaussian estimate of the PSF that represents the effects of the atmosphere and the telescope. A convolved Gaussian function has the form

$$G_c(r, a, c) = \frac{a^2}{(a^2 + c^2)} G(r, \sqrt{a^2 + c^2}) . \quad (7)$$

With this notation the observed bright point contrast function can be written directly as

$$\mathrm{DG}(r, a, b, c, \alpha, \delta) = (\alpha + \delta)G_c(r, a, c) - \delta G_c(r, b, c) . \quad (8)$$

The observed peak contrast is

$$\mathrm{DG}(0, a, b, c, \alpha, \delta) = (\alpha + \delta)[a^2/(a^2 + c^2)] - \delta[b^2/(b^2 + c^2)] . \quad (9)$$

The peak contrast can be negative with respect to the local Sun intensity. However, for a point to appear bright it only needs to be brighter than its immediate neighborhood. As a consequence, there may be many bright points in an image that do not have positive contrast with respect to tops of granules. Using equation (6), the PSF HWHM, $c_0$, that causes the observed central contrast to be zero can be written as

$$c_0^2 = b^2\left(\frac{q}{1 - q}\right) . \quad (10)$$

For $c_0$ to be real requires that $q < 1$, and thus the integrated contrast by condition (5) must be negative, which, of course, must be true. If $q > \frac{1}{2}$, then $c_0 < b$.

Because of the analytic form of the DG function it is straightforward to develop closed-form expressions for the position of the minimum contrast, the contrast at the minimum, the peak-to-valley (PV) contrast amplitude, and the contrast at the HWHM. These expressions are complicated, however, and they will not be reproduced here.

If equation (8) is written with the change in variables,

$$\delta = p\alpha , \quad (11)$$

then

$$\mathrm{DG}(r, a, b, c, \alpha, p) = \alpha[(l + p)G_c(r, a, c) - pG_c(r, b, c)] . \quad (12)$$

From the form of equation (12), DG functions scale with $\alpha$ for fixed $p$. Hence, the ratio of the peak contrast to PV contrast, the location of the minimum, and the HWHM are functions of the seeing, core, and surround HWHM value, and the ratio $\alpha/\delta$.

Our definition of the DG function has five free parameters. However, one of the parameters, the width of the PSF, cannot be determined because it always occurs in combination with the widths of the core and surround. We assume the PSF HWHM is very close to that of a Gaussian fit to the Airy function for a 48 cm telescope. Assuming a greater width for the PSF causes the estimates of the intrinsic core width to decrease and the intrinsic core brightness to increase significantly.

We can measure the HWHM of the DG core and dark surround, the position of the minimum ring around the core, the PV amplitude of the bright point, and the contrast at the peak from the data. Therefore, in principle, we can determine the model parameters to obtain the intrinsic contrast profiles. But the Sun is more complex than our model, and a number of effects such as the presence of lanes, irregular surrounding granulation, and other nearby bright points make the precise estimate of the intrinsic solar structures difficult. However, many of these problems can be minimized by selection of relatively isolated bright points.

Equation (8) describes a cylindrically symmetric DG as a function of the distance from its center. It can be generalized to make the local surroundings more "lane-like" by modeling the surround with different surround HWHMs, $b_x$ and $b_y$, in the $x$ and $y$ directions, where the $x$ direction is defined as across the lane and the $y$ direction is defined as along the lane. The model for a cylindrically symmetric bright point with an elongated surround is,

$$\mathrm{DG}_{\mathrm{lane}}(x, y, a, b_x, b_y, c, \alpha, \delta) = (\alpha + \delta)G_c[(x^2 + y^2)^{1/2}, a, c] - \delta G_c(x, b_x, c)G_c(y, b_y, c)[b_x b_y(b_x^2 + c^2)^{1/2}(b_y^2 + c^2)^{1/2}] . \quad (13)$$

### 3.2. *Fitting of the Model to Isolated Bright Points*

Shown in Figure 3 are four areas from Figure 1 that are 65 pixels (4.″08) square with a bright point at their center. These examples were chosen because they are isolated bright points at vertices in the granulation pattern. Figure 4 shows contrast traces in the $x$ direction through the center of each of these bright points (*thick lines*). The zero contrast level was adjusted to the plateaus of the granules on both sides of each bright point. Shown as thin lines in the figure are fits to the contrast traces using equation (8). The panels of Figure 4 contain the values of $a$, $b$, $\alpha$, and $\delta$ for the fit. For all the fits we have assumed $c = 0.''095$, which is close to the HWHM of the PSF of a perfect telescope. (The Gaussian fit to the theoretical transfer function of a 48 cm diameter, unobscured telescope has a HWHM = 0.″093.) These four bright points have a core HWHM, $a$, of 0.″105 or less while their intrinsic contrasts, $\alpha$, are all less than 0.″52. In all cases, the intrinsic depth, $\delta$, is greater than 0.33, which is greater than that of a normal intergranular lane whose intrinsic contrast ranges between −0.10 and −0.25.

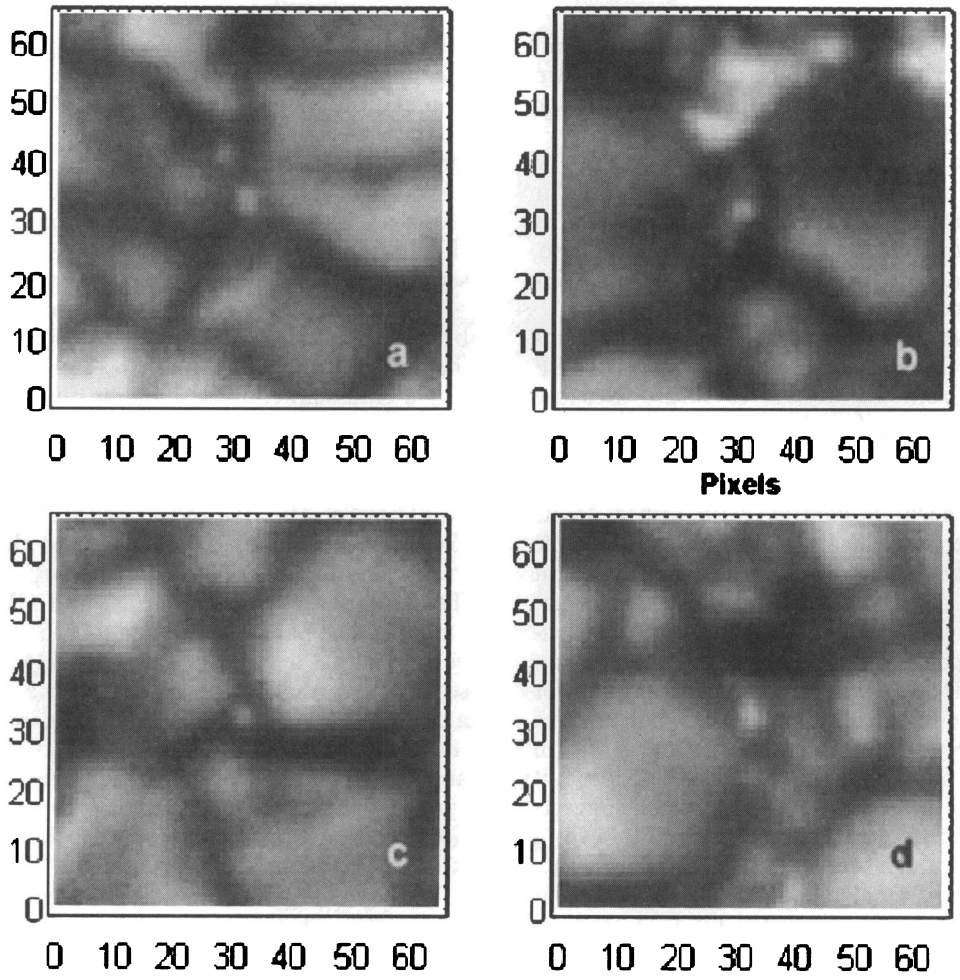


FIG. 3.—Four 65 × 65 pixel (4.″09) square regions, each centered on a bright point in relatively quiet Sun

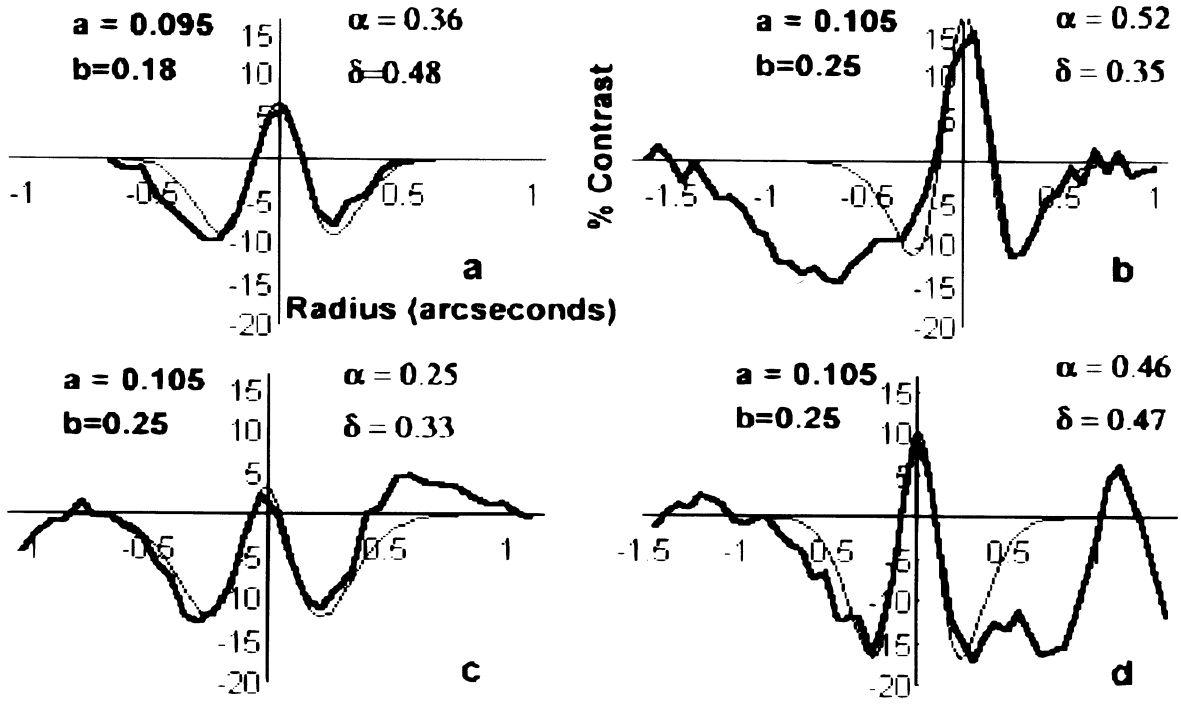


FIG. 4.—Traces (*thick lines*) in the *x* direction through the centers of each of the four bright points of Fig. 3 versus distance from the center of the bright point in arcseconds. DG fits (*thin lines*) to the data. Displayed on each panel are the fitting parameters for the DG.

To illustrate some of the properties of our bright point model we take the contrast profile of the bright point shown in Figure 3*a* as an example. Our fit to the horizontal trace (Fig. 4*a*) to this bright point has an observed HWHM = 0".10, an observed peak contrast of 0.067, an observed PV contrast amplitude of 0.157, and $c = 0''.095$. This particular bright point is below average in PV contrast. However, it is neither the smallest nor dimmest example in our data. Also, note that the inferred core width, $a = 0''.095$, is only 5% smaller than the observed width.

Figure 5*b* simulates the effect of seeing. It shows how this model bright point diminishes in contrast as the PSF HWHM increases from $c = 0''.095$ to 0".25. Because $(b^2 - a^2)/a^2 = 2.59$, $\alpha/\delta = 0.84$, and $q = 0.33$, the integrated contrast of this bright point is negative (eq. [5]). From equation (10), for $c > 0''.125$, which is less than $b$, the peak brightness will have negative contrast with respect to its local surroundings. Because the PSF width is less than the lane width, normal lanes will still be visible as the bright point vanishes. The figure shows the peak contrast is negative at $c = 0''.15$, and by $c = 0''.20$ the bright point has essentially zero PV amplitude and would not be detectable in an image. Shown in Figure 5*a* are inferred contrast profiles for the case of a perfect telescope of 96 cm ($c = 0''.0475$) and the intrinsic structure ($c = 0''$). Comparison of the plots in Figures 5*a* and 5*b* demonstrates that the HWHM does not change significantly with the PSF HWHM, which suggests that even with a larger telescope the bright points seen in Figure 1 would not get much smaller in size.

A diffraction limited 24 cm telescope has $c = 0''.186$ at $\lambda 4305$. Therefore, in an image produced by a 24 cm telescope in perfect seeing, all of the example bright points shown in Figure 4 would have negative central peaks and very small PV amplitudes, and thus be very difficult to recognize. For example, the nearly diffraction limited granulation images taken with the 30 cm SOUP telescope on the Spacelab 2 mission contained few bright points. This suggests the 48 cm Swedish Vacuum Solar Telescope would miss bright points that are smaller than 0".05 HWHM. However, if there are such smaller features on the Sun they should suddenly appear with a one meter diameter telescope performing at the diffraction limit.

It is instructive to compare the results obtained by fitting bright points with DG functions to the more traditional method of fitting with Gaussians. For structures that have a single Gaussian contrast function the observed HWHM is the square root of the sum of the squares of the intrinsic and PSF HWHM values. To match the observed HWHM and PV contrast of our example requires that a Gaussian bright point have $a = 0''.0312$ and $\alpha = 1.615$. Thus, the width of the Gaussian is a factor 3.0 smaller and the central contrast more than a factor of 3.6 greater than required to produce the same observed PV contrast and HWHM with a DG function. The parameters $a$ and $\alpha$ of the single Gaussian are very sensitive to the measured HWHM and the assumed seeing. Nevertheless, for features with a Gaussian shape on a uniform background to appear in an image with sizes near the telescope resolution requires that the intrinsic structures approach point sources, and, thus, must be very bright and small. That is, the single Gaussian contrast profile assumption for Solar bright points implies the existence of unrealistically bright and small structures.

We have illustrated above that single and double Gaussian functions behave quite differently with changes in the HWHM of the PSF. The plots in the bottom row of Figure 5 show how single Gaussian functions with the same

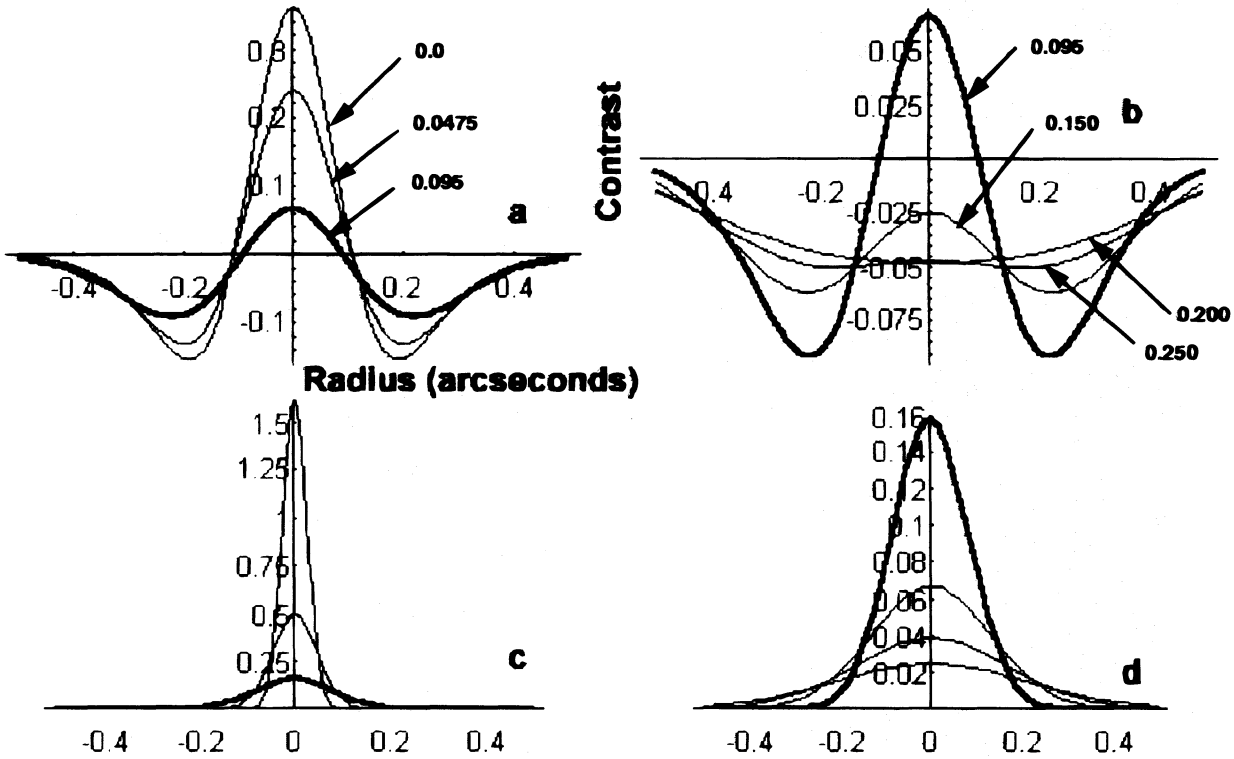


FIG. 5.—Double Gaussian functions versus radius (top) for the DG model of the bright point in Fig. 3*a* for $c = 0''.0$, 0".0475, and 0".095 (*heavy*) (*a*) and for $c = 0''.095$ (*heavy*), 0".150, 0".200, and 0".250 (*b*). Single Gaussian functions versus radius (bottom) for a Gaussian model that has the same HWHM and PV contrast as the bright point in Fig. 3*a* for $c = 0''.0$, 0".0475, and 0".095 (*heavy*) (*c*) and for $c = 0''.095$ (*heavy*), 0".150, 0".200, and 0".250 (*d*).

observed HWHM and contrast amplitude as the DG at $c = 0''.095$ change with $c$. Note that the DG bright point is gone when $c = 0''.200$ (Fig. 5*b*), while a single Gaussian should easily be detectable with a central contrast of 0.065 (Fig. 5*c*). In Figure 6 are simulated images of the DG (*top row*) and single Gaussians (*bottom row*) bright point models. It is clear from Figure 6 that a DG bright point becomes a "dark point" when $c = 0''.20$, while the single Gaussian is still visible.

Figure 7 contains plots of the PV-observed contrast amplitude versus PSF HWHM for our example DG and the single Gaussian with the same HWHM and PV contrast at $c = 0''.095$. The right-hand panel shows on an expanded scale the relative behavior for $c > 0''.095$. The DG bright point disappears much more rapidly with increase HWHM of the PSF than the single Gaussian structure. Conversely, with the decrease of the HWHM of the PSF, the Gaussian bright point would rapidly grow brighter than a DG bright point. Together Figures 5–7 demonstrate a mathematical model that can explain why bright points are seldom visible when the seeing is worse than $0''.3$. This result can be checked with the real data. In Figure 8 we have blurred the example bright in Figure 3*a* to $c = 0''.150$, $0''.200$, and $0''.250$; just as predicted the bright point rapidly disappears.

It is initially surprising that the observed HWHM DG function is relatively insensitive to the width of the PSF. Figure 9 shows the observed HWHM versus $c$ for our model DG bright point. The plot shows that for $c > 0''.1$ the observed HWHM will be smaller than the PSF. Note that for seeing plus telescope smearing greater than $0''.11$ the

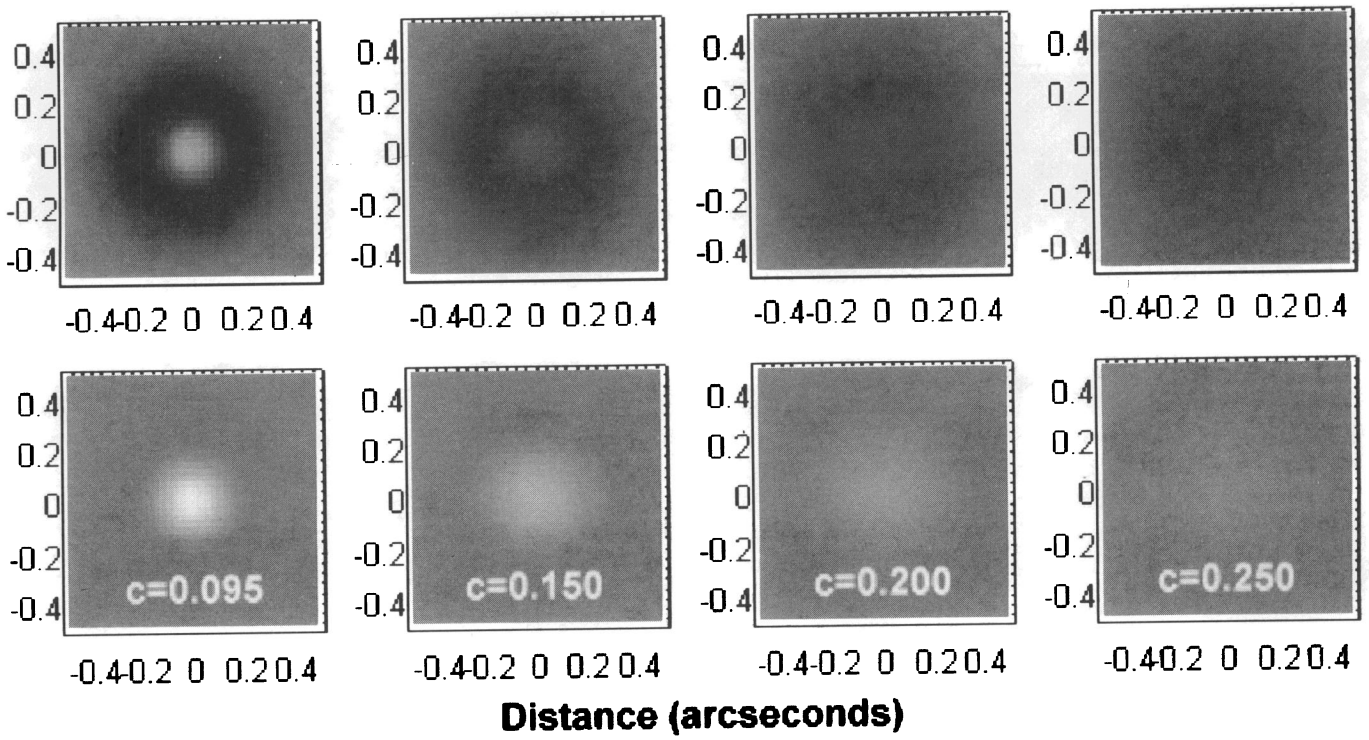


FIG. 6.—Top row shows the two-dimensional appearance of some of the DG functions in Fig. 5*b*, and the bottom row shows the single Gaussian functions plotted in Figure 5*d*. The density range of all the images is the same.

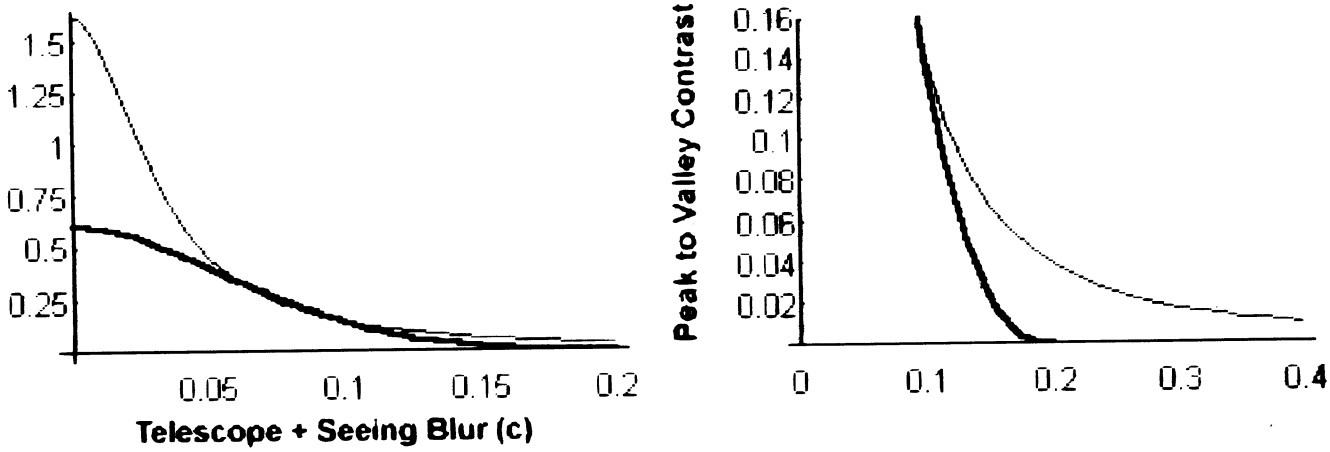


FIG. 7.—Observed PV contrast versus PSF HWHM for single and double (*thick line*) Gaussian functions. The parameters of both functions have been adjusted to have an observed PV contrast of $0''.157$ and a HWHM = $0''.10$ when $c = 0''.095$. The right-hand panel shows the observed contrast on an expanded scale.

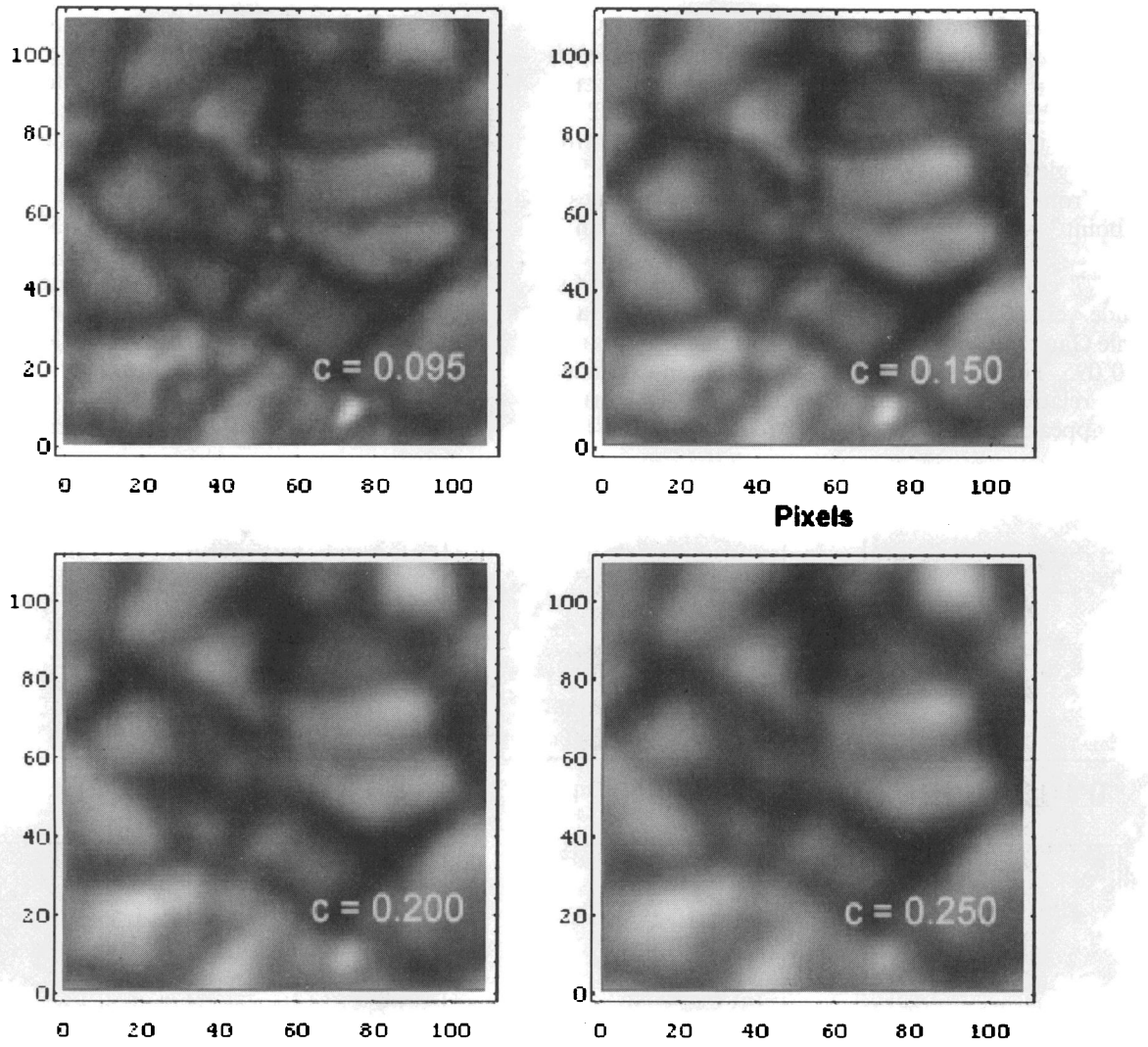


FIG. 8.—Region shown in Figure 3*a* blurred so that $c = 0''.095$, $0''.150$, $0''.200$, and $0''.250$. The region shown is 110 pixels ($6''.91$) square.

observed HWHM actually drops with increasing HWHM of the PSF. The reason for this unexpected behavior is that both the surround and the core smear simultaneously, and the inward smear of the surround tends to cancel the outward smear of the core. This behavior does not violate any fundamental relations between aperture diameter and resolution. The highest spatial frequency passed by a telescope of diameter $D$ is $\lambda/D$, so that the FWHM of a single peak of this wave is $\lambda/(2D)$, which is much smaller than the $1.22\lambda/D$ classical diffraction limit.

The most reliable observable parameters of the bright points are the HWHM of the core and the PV contrast of

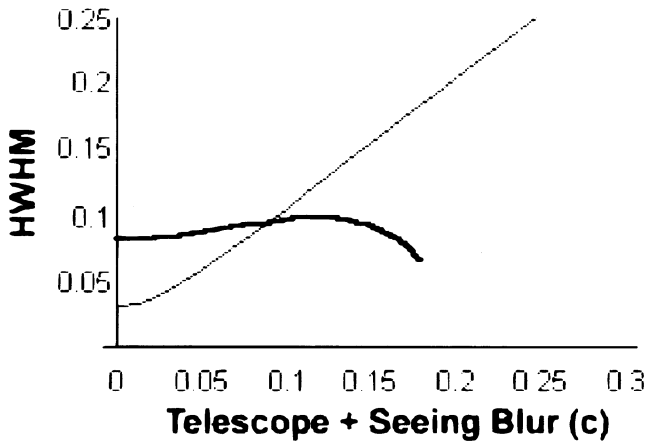


FIG. 9.—HWHM versus PSF HWHM for single (*thin line*) and double (*thick line*) Gaussian functions. The parameters of both functions have been adjusted to have an observed contrast of 0.35 and a HWHM = $0''.10$ when $c = 0''.095$.

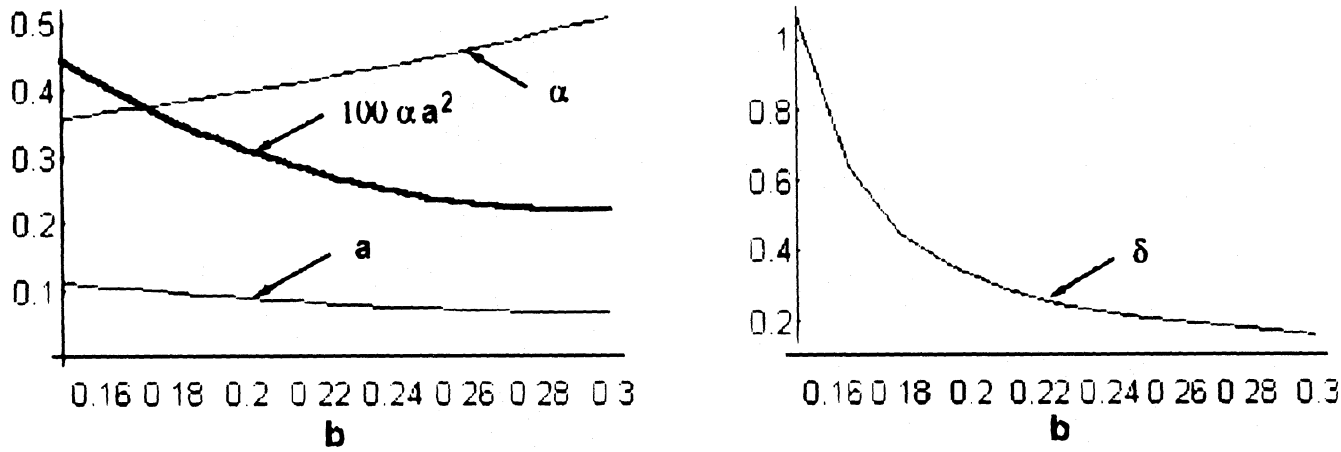


FIG. 10.—Plots of values of $a$, $\alpha$, and $100a^2\alpha$ (left) and $\delta$ (left) versus $b$. The values are obtained for observed profiles with HWHM = 0.″10, peak contrast = 0.067, and peak contrast to PV contrast amplitude = 0.157.

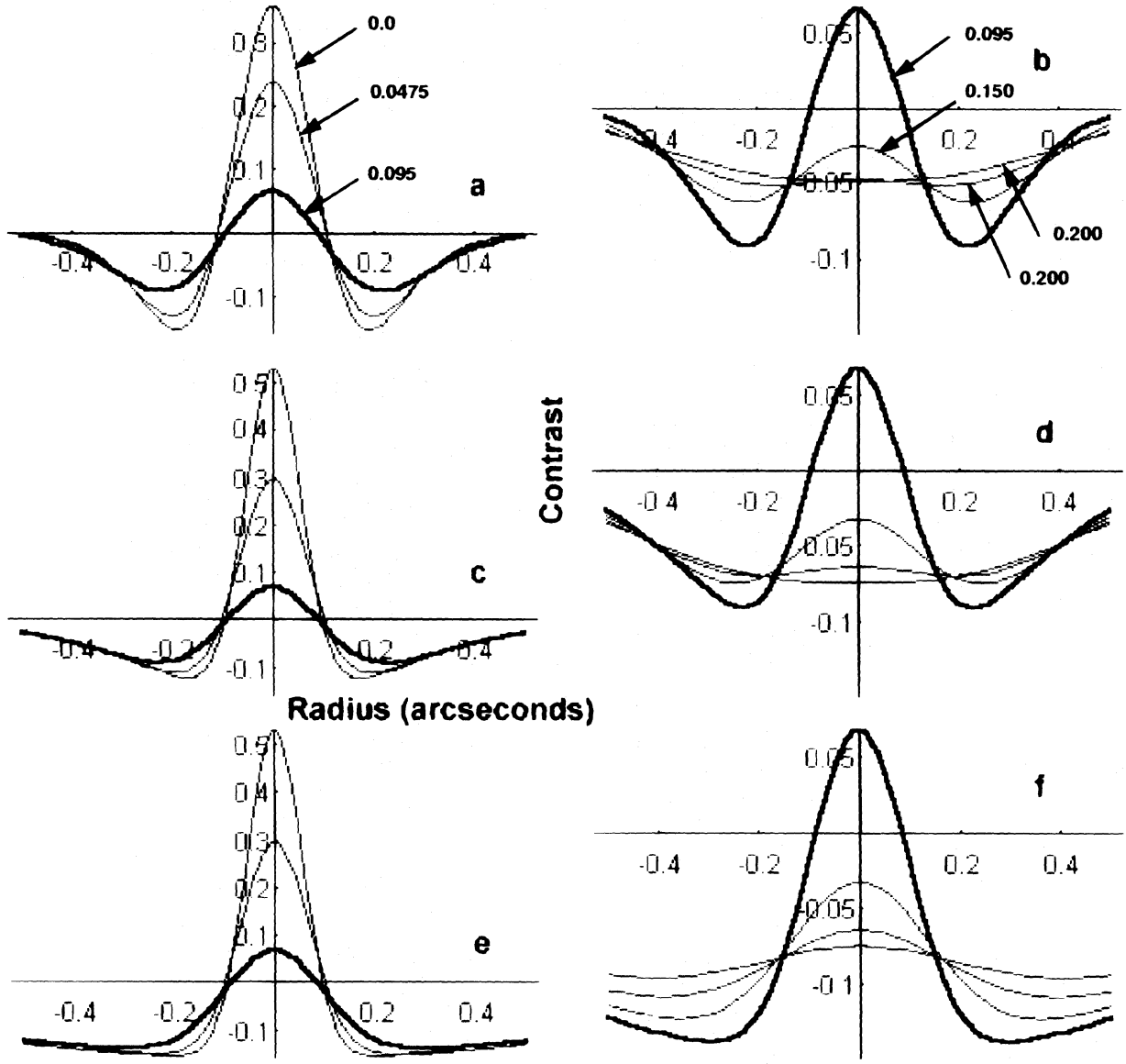


FIG. 11.—Plots in (*a*) and (*b*) show duplicate plots of 5*a* and *b*, for reference. The other panels in the figure show DG contrast functions for a cylindrically symmetric bright point in a 1–3 lane, $b_x = 0.3$, $b_y = 9$, versus radius for a Gaussian model that has the same HWHM and PV contrast in the $x$ direction as the bright point in Fig. 3*a* for $c = 0.″0$, 0.″0475, and 0.″095 (*heavy*) (*c*) and for $c = 0.″095$ (*heavy*), 0.″150, 0.″200, and 0.″250 (*d*) in the $y$ direction in (*e*) and (*f*).

the bright point, and the least reliable is the HWHM of the surround. To develop some quantitative estimates of our fitting procedures we fixed the value of the observed core HWHM, the peak contrast, and the PV contrast then varied $b$, the HWHM of the surround, and then solved for $a$, $\alpha$, and $\delta$. Qualitatively, increasing $b$ will decrease $a$ and increase $\alpha$, because as $b$ increases the single profile approaches the Gaussian form. Shown in the left-hand panel of Figure 10 are plots of $a$, $\alpha$, and 100 $\alpha a^2$ versus $b$ for our example bright point, with observed HWHM = 0".10, peak contrast = 0.067, and PV contrast −0.157. The right-hand panel shows $\delta$ versus $b$. If we can estimate $b$ to 10%, these calculations indicate that we can infer $a$ and $\alpha$ to about 4.5% and 9%, respectively. Note that as $b$ increases $\alpha a^2$ decreases.

### 3.3. *Effect of Intergranular Lanes*

In the calculations above we have used a circularly symmetric model for bright points (eq. [9]), which is a reasonable approximation for isolated bright points in vertices in the granulation pattern. Isolated bright points are seldom seen in intergranular lanes in quiet Sun, which is not surprising because the flow field associated with granulation collects magnetic fields into sinks that define the vertices in the granulation pattern (Simon et al. 1988). Nonetheless, the calculations above suggest that when $b$ is greater than 0".25 the value of the intrinsic contrast of the surround Gaussian is on the order of −0.25, which is comparable to the intrinsic contrast estimated for intergranular lanes. Most lane regions are well fitted by a negative Gaussian with a HWHM = 0".3 and a contrast of −0.18. This suggests that an explanation of the appearance of many of our bright points is that they are cylindrically symmetric Gaussian shaped structures in Gaussian shaped lanes (eq. [13]). The bright point shown in Figure 3*a*, however, is a clear example that requires a darker surround than normally occurs in lanes. Shown in Figure 11 are plots of the contrast of a cylindrical bright point and surround (*top*) and a cylindrical bright point in a lane with a 1–3 aspect ratio ($b_x$ = 0.3, $b_y$ = 0.9) versus $x$ (*middle*) and $y$ (*bottom*) for the ranges in $c$ used in Figure 5. At $c$ = 0".095 the parameters of the lane model are chosen so that the HWHM, the peak contrast, and the PV contrast are all the same, as with the cylindrically symmetric case in the direction across the lane ($x$-axis). Along the lane ($y$-axis) the surroundings of the bright core are much darker than across it, as can be seen by comparison of the middle and bottom panels. Because of the asymmetric contrast pattern, the HWHM of the bright point is greater along the lane than perpendicular to it. However, this does not give rise to an easily noticed asymmetric appearance to the bright points in images, because contrast contours are nearly circular at contrasts above the HWHM in the $x$ direction.

## 4. DISCUSSION AND CONCLUSIONS

We have demonstrated that the properties of the immediate neighborhood of a small bright structure are critical to both its observability and the interpretation of its intrinsic characteristics. The inclusion of a dark surround as a fundamental feature of the bright point can explain the observation that, although small bright points have high contrast in the very best images, they are seldom seen in images with resolutions on the order of 0".3 or worse. The modeling efforts described above should be regarded as qualitative because of the significant variations in the size and depth of the vertices and lanes in the granulation pattern. In addition, results are derived assuming Gaussian profiles for the structures and for the telescopic and atmospheric blur. Although these assumptions are not precisely correct, the general character of our results should not change significantly when more detailed PSFs and input profiles are used. With these caveats in mind, the simple DG models predict that:

1. Most of the bright points seen in both G band and continuum images at a resolution of 0".2, will appear as dark structures when observed with a resolution of 0".4 or worse. This means that most of the quiet Sun bright points in both CH and continuum images at disk center have a negative integrated contrast.
2. Because of the sensitivity of the observed contrast amplitude to resolution, there probably are bright points on the Sun that we cannot detect with a 48 cm telescope, even under perfect seeing conditions, because they are smaller than 0".05 HWHM.
3. The intrinsic cores of bright points are, in general, dimmer and broader than those inferred from models that neglect the shape of the immediate surroundings.
4. If detected, the HWHM of DG bright points is nearly insensitive to the value of the resolution, therefore is a reasonable estimator for the intrinsic size of the core.
5. Objects can be observed with FWHM's smaller than the classical Rayleigh criteria ($1.22\lambda/D$) "diffraction limit" of a telescope. FWHMs as small as $\lambda/(2D)$ are, in principle, detectable. We have found structures smaller than $\lambda/D$ in both G band and continuum images.

Based on the DG models, we have some confidence in the detection of structures with intrinsic core as small as 0".07 in radius or 100 km in diameter in Figure 1. Because three image pixels correspond to 0".188, and it is difficult to estimate FWHMs much less than three pixels, cores much less than 0".07 HWHM probably cannot be reliably inferred from measurements on this image. Since this image is probably at the limit of what can be achieved with a 0.5 m telescope, the detection of smaller magnetic features will require diffraction limited meter-class or larger telescopes. Given the rarity of near diffraction limited images at ground-based observatories with a 0.5 m aperture optics, higher resolution imagery will require either active optics or phase diversity techniques for ground-based telescopes or the seeing free environment of space (Title 1993).

The relative lack of expansion of the continuum sites of magnetic flux tubes, bright points, with PSF implied by the DG modeling can explain why magnetogram features appear larger in magnetograms than in the RCP and LCP pairs from which they are constructed. The Stokes $V$ polarization signal caused by a small flux tube usually occurs against a locally flat surround, and hence the HWHM of the flux tube grows like the square root of the sum of the squares of the seeing and telescope spread widths, whereas the apparent size of the bright point sites of the magnetic flux tubes have nearly constant HWHM's regardless of seeing because they are surrounded by dark rings. In addition, the intrinsic size and the observed size of the bright points are roughly comparable in Figure 1, which suggests that the majority of the magnetic field structures should appear to be on the order of the square root of two larger than the bright points.

The fact that most continuum bright points, if observed at low resolution near disk center, have a contrast that is less than the mean photosphere, can explain the results of Hirayama and his collaborations who found that the locations of magnetic field near disk center have lower than average solar intensity. Nevertheless, the locations of magnetic field still may make a positive contribution to the solar flux because in the absence of fields the intergranular lanes in which the fields are found might have been even darker.

The evolution of bright points has not been mentioned above. Movies showing bright point evolution are currently under study and our initial conclusions are in Berger & Title (1995b). We gratefully acknowledge useful discussions with Drs. D. S. Acton, Hirayama, Sakurai, Scharmer, Schrijver, Shine, Simon, and Tarbell. One of us (A. M. T.) was a guest of the Ministry of Education, Science, and Culture of Japan at the National Observatory of Japan when much of this work was done, and he gratefully acknowledges their support. This research has been supported in part by NASA contract NAS 8-39747, Lockheed Independent Research Funds, and grants from the Royal Swedish Academy of Sciences.

## REFERENCES

Berger, T. E., Shine, R. A., Schrijver, C. J., Tarbell, T. D., Title, A. M., & Scharmer, G. B. 1995a, ApJ, 454, 531
Berger, T. E., Shine, R. A., Tarbell, T. D., Title, A. M., & Scharmer, G. B. 1994, AGU Abs, SH11A-09
———. 1995b, ApJ, submitted
Chapman, G. A. 1970, Sol. Phys., 13, 78
Chapman, G. A., & Sheeley, N. R., Jr. 1968, Sol. Phys., 5, 442
deBoer, C. R., & Kneer, F. 1992, A&A, 139, 435
Dunn, R. B., Mann, G. R., & Simon, G. W. 1973, BAAS, 4, 381
Dunn, R. B., & Zirker, J. B. 1974, Sol. Phys., 33, 281
Hirayama, T., Hamana, S., & Mizugaki, K. 1985, Sol. Phys., 99, 43
Knolker, M., Schussler, M., & Weisshaar, E. 1988, A&A, 202, 275
Lawrence, J. K., Topka, K. P., & Jones, H. P. 1993, J. Geophys. Res., 98, A11, 18, 911
Mehltretter, J. P. 1974, Sol. Phys., 38, 43
Muller, R. A. 1985, Sol. Phys., 100, 237
Muller, R. A. & Keil, S. L. 1983, Sol. Phys., 119, 229
Muller, R. A., Roudier, T., Vigneau, J., & Auffret, H. 1994, A&A, 283, 232
Nishikawa, J. 1990, ApJ, 359, 235
Nishikawa, J. & Hirayama, T. 1990, Sol. Phys., 127, 211
Sheeley, N. R., Jr. 1969, Sol. Phys. 9, 347
Simon, G. W., Title, A. M.,. Topka, K. P., Tarbell, T. D., Shine, R. A., Ferguson, S. H., Zirin, H., & the SOUP Team 1988, ApJ, 327, 964
Spruit, A. C., & Zwaan, C. 1981, Sol. Phys., 61, 363
Title, A. M. 1993, ESA SP-1157, 161
Title, A. M., Topka, K. P., Tarbell, T. D., Schmidt, W., Balke, C., & Scharmer, G. B. 1992, ApJ, 393, 782
Topka, K. P., Tarbell, T. D., & Title, A. M. 1992, ApJ, 396, 351
Zhang, Y., & Engvöld, O. 1993, Sol. Phys., 144, 1